



Residual Temperature Bias Effects in LIMS Stratospheric Ozone and Water Vapor

Ellis Remsberg¹, V. Lynn Harvey², Arlin Krueger³, and Murali Natarajan¹

¹Science Directorate, NASA Langley Research Center, 21 Langley Blvd, Mail Stop 401B,
Hampton, VA 23681, USA

²Laboratory for Atmospheric and Space Physics, University of Colorado Boulder, 3665
Discovery Drive, Boulder, CO 80303, Colorado, USA

³Emeritus Senior Scientist, Code 614 Atmospheric Chemistry and Dynamics Laboratory, NASA
Goddard Space Flight Center, Greenbelt, MD 20771, USA

Correspondence to: Ellis Remsberg (ellis.e.remsberg@nasa.gov)



20 Abstract

21 The Nimbus 7 Limb Infrared Monitor of the Stratosphere (LIMS) instrument operated from
22 October 25, 1978, through May 28, 1979. Its Version (V6) profiles were processed and archived
23 in 2002. We present several diagnostic examples of the quality of the V6 stratospheric ozone
24 and water vapor data based on their Level 3 zonal Fourier coefficient products. In particular, we
25 show that there are small differences in the ascending (A) minus descending (D) orbital
26 temperature-pressure or T(p) profiles (their A-D values) that affect (A-D) ozone and water vapor.
27 Systematic A-D biases in T(p) can arise from small radiance biases and/or from viewing
28 anomalies along orbits. There can also be (A-D) differences in T(p) due to not resolving and
29 correcting for all of the atmospheric temperature gradient along LIMS tangent view-paths. An
30 error in T(p) affects the retrievals of ozone and water vapor through: (1) the Planck blackbody
31 function in forward calculations of limb radiance that are part of the iterative retrieval algorithm
32 of LIMS, and (2) the registration of the measured LIMS species radiance profiles in pressure-
33 altitude, particularly for the lower stratosphere. We evaluate V6 ozone profile biases in the
34 upper stratosphere with the aid of comparisons against a monthly climatology of UV-ozone
35 soundings from rocketsondes. We also provide results of time series analyses of V6 ozone,
36 water vapor, and potential vorticity for the middle stratosphere to show that their average (A+D)
37 V6 Level 3 products provide a clear picture of the evolution of those tracers during northern
38 hemisphere winter. We recommend that researchers use the average V6 Level 3 data for their
39 science studies of stratospheric ozone and water vapor wherever diurnal variations of them are
40 unexpected. We also point out that the present-day Sounding of the Atmosphere using
41 Broadband Emission Radiometry (SABER) experiment is providing measurements and retrievals
42 of temperature and ozone, which are essentially free of any anomalous diurnal variations.

43



44 **1 Introduction and objectives**

45 The historic Nimbus 7 Limb Infrared Monitor of the Stratosphere (LIMS) experiment provided
46 data on the middle atmosphere from October 25, 1978, through May 28, 1979, for scientific
47 analysis and for comparisons with atmospheric models (Gille and Russell, 1984). Remsberg et
48 al. (2007) describe characteristics of the ozone profiles of the LIMS Version 6 (V6) dataset.
49 Notably, V6 corrects for a high ozone bias in the lowermost stratosphere of the previous Version
50 5 (V5) profiles, as shown by comparisons of the V6 profiles with ozonesonde data in Remsberg
51 et al. (2007; 2013). Remsberg et al. (2009) also reported on improvements in the profiles and
52 distributions of V6 water vapor (H_2O) within the lower stratosphere, where temperature and
53 interfering radiances from the oxygen continuum are more accurate than in the processing of V5.

54

55 Frith et al. (2020) reported on modeled estimates of diurnal ozone variations, as a function of
56 latitude, altitude, and season. In general, their modeled results are in accord with observed ozone
57 variations from both satellite ultraviolet (uv) and microwave measurements. However, the ozone
58 distributions from the infrared measurements of LIMS show some anomalously large day/night
59 differences in the middle stratosphere (Remsberg et al., 1984; 2007). LIMS ozone and H_2O are
60 quite sensitive to small biases of the LIMS temperature versus pressure, or $T(p)$, due to nonlinear
61 effects of the Planck blackbody function in forward radiance calculations that are part of the
62 LIMS retrieval algorithm (Gille et al., 1984; Remsberg et al., 2004). Consequently, temperature
63 bias is the largest source of ozone and H_2O error, by far, although such bias effects from $T(p)$ are
64 hard to verify from correlative comparisons of individual profiles. The LIMS orbital line-of-site
65 to its tangent layer is nearly in a meridional direction or along horizontal temperature gradients
66 (Gille et al., 1984). Roewe et al. (1982) showed that it is important to incorporate line-of-sight
67 $T(p)$ gradient corrections for the LIMS species retrievals. While the LIMS algorithm makes first
68 order corrections for $T(p)$ gradients, residual bias effects are still apparent in the V6 species
69 distributions.

70

71 This study considers distributions of LIMS temperature, ozone, and H_2O and plots of their
72 ascending (A) minus descending (D) orbital differences (A-D), as diagnostics for the effects of



73 residual bias errors in T(p). We evaluate those effects using plots of the LIMS V6 Level 3
 74 (mapped) products (Remsberg and Lingenfelter, 2010) and their monthly zonal mean
 75 distributions that are part of the SPARC Data Initiative (SPARC, 2017). Section 2 gives a brief
 76 review of characteristics of the V6 ozone, temperature, and H₂O and their retrieval algorithms.
 77 Section 3 reviews the measurement, retrieval, and day/night differences for temperature. Section
 78 4 relates small temperature biases to the anomalous A-D values in the LIMS monthly species
 79 distributions for March 1979. Section 5 compares V6 daytime ozone with rocketsonde UV-filter
 80 ozone (ROCOZ) profile data for the upper stratosphere and lower mesosphere. We interpret the
 81 comparisons according to their respective error estimates and by examining the profiles in the
 82 context of hemispheric maps of the surrounding ozone and temperature fields from the Level 3
 83 product. Section 6 contains results of time series of northern hemisphere (NH) distributions of
 84 V6 ozone and H₂O on the 850 K potential temperature surface (~10 hPa), as indications of the
 85 quality of those V6 data. Section 7 summarizes our findings about V6 ozone and H₂O and our
 86 recommendations for scientific studies of them. We also point out why the follow-on, Sounding
 87 of the Atmosphere using Broadband Emission Radiometry (SABER) experiment is providing
 88 measurements and retrievals of temperature and ozone that are of better quality than from LIMS.

89

90 **2 Characteristics of the V6 Level 3 ozone, temperature, and water vapor**

91 *2.1 Daily mapped data*

92 The V6 algorithm accounts for low-frequency spacecraft motions that affect how the LIMS
 93 instrument views the horizon and the subsequent registration of its measured radiance profiles in
 94 pressure-altitude (Remsberg et al., 2004). Retrieved ozone, temperature, and geopotential height
 95 (GPH) profiles extend from 316 hPa to ~0.01 hPa and have a point spacing of ~0.88 km with a
 96 vertical resolution of ~3.7 km. H₂O, nitric acid vapor (HNO₃), and nitrogen dioxide (NO₂) data
 97 are limited to the stratosphere (~100 hPa to 1 hPa). Processing of the original V5 T(p) profiles
 98 occurred at a rather coarse vertical point spacing of ~1.5 km and for every ~4 degrees of latitude.
 99 Retrievals for V6 occur at every ~1.6 degrees of latitude along orbits and resolve the horizontal
 100 temperature structure better. However, the horizontal line-of-sight T(p) gradients for both the
 101 V5 and V6 processing algorithms are from daily maps of the combined V5 (A+D) temperature
 102 fields on pressure surfaces.



103

104 The mapping of the V6 profiles to a Level 3 product occurs at 28 vertical levels, as opposed to
 105 just 18 levels for V5. The sequential-estimation mapping algorithm for V6 (Remsberg and
 106 Lingenfelter, 2010) employs a shorter relaxation time of about 2.5 days for its zonal wave
 107 coefficients, compared with ~5 days for V5. The mapping algorithm is also insensitive to the
 108 very few large, unscreened ozone mixing ratio values within the lower stratosphere, as noted in
 109 Remsberg et al. (2013, Fig. 1a). LIMS made measurements with a duty cycle of up to 11 days
 110 on and 1 day off, and the mapping algorithm interpolates the profile data in time to provide a
 111 continuous, 216-day set of daily zonal coefficients. The daily maps provide a spatial context for
 112 the individual V6 profiles and are helpful for interpreting comparisons with auxiliary data sets,
 113 especially during dynamically disturbed periods.

114

115 *2.2 Monthly zonal average V6 ozone, temperature, and water vapor*

116 We generated monthly zonal mean distributions from the daily Level 3 files of temperature and
 117 species (ozone, H₂O, HNO₃, and NO₂) and supplied them to the SPARC Data Initiative or
 118 SPARC-DI (SPARC, 2017). Since the V6 ozone for SPARC-DI extended up to only the 0.1-hPa
 119 level (~64 km), Figure 1 updates the combined (A+D), monthly ozone for March 1979 to its
 120 highest level of about 0.015 hPa (~75 km). Retrieved V6 daytime ozone in Fig. 1 has a large
 121 positive bias throughout the mesosphere because the LIMS algorithms do not account for non-
 122 local thermodynamic equilibrium (NLTE) effects from both ozone (Solomon et al., 1986;
 123 Mlynchak and Drayson, 1990) and CO₂ (Edwards et al., 1996; Manuilova et al., 1998).
 124 However, the V6 nighttime ozone is essentially free of NLTE effects below about the 0.05-hPa
 125 level. We also screened the SPARC-DI product of daily zonal mean ozone values (<0.1 ppmv)
 126 near the tropical tropopause, as recommended in Remsberg et al. (2013). This study focuses on
 127 the quality of the V6 ozone in the stratosphere.

128

129 Figure 1 shows that ozone has largest mixing ratios at about 10 hPa near the Equator (~10.8
 130 ppmv), decreasing sharply above and below that level. Maximum mixing ratios at the middle to
 131 high latitudes occur closer to 3 hPa, due to larger zenith angles and longer paths of the uv light



for the production of its atmospheric ozone. Remsberg et al. (2007) compared V6 ozone and Solar Backscatter UltraViolet (SBUV) Version 8.0 ozone and reported that V6 ozone is larger (4 to 12%) in the upper stratosphere, although the differences are within the combined errors of V6 and SBUV. However, the monthly comparisons at 4 hPa indicate that the differences increased from November to May. Sun and Leovy (1990, their Fig. 1) also compared Equatorial ozone time series from LIMS and SBUV, and they found that their monthly differences for the upper stratosphere changed with the descent of the semi-annual oscillation (SAO). Most likely, LIMS and SBUV do not resolve the vertical response of ozone to the SAO equally well.

140

Figure 2 shows the March zonal mean V6 T(p) distribution from SPARC-DI. Monthly T(p) extends to near the 0.01-hPa level and has values every 5° of latitude. T(p) has a maximum value of about 275 K at the stratopause and minimum values approaching 195 K near the mesopause and at the tropical tropopause. Radiances from the two 15-micrometer CO₂ channels for retrievals of T(p) are free of NLTE effects below about the 0.05-hPa level (~70 km) (Lopez-Puertas and Taylor, 2001). Estimates of a bias in V6 T(p) are in Table 1 (row 2), according to the error simulations of Remsberg et al. (2004). Estimates of bias errors for ozone due to those T(p) errors are in Table 1 (row 3); a positive bias in temperature leads to a negative bias in retrieved ozone (and in H₂O) via the effect of the Planck function on radiance calculations. In principle, one may also infer the quality of the V6 temperatures based on independent estimates of the quality of the retrieved ozone. Table 1 (last row) compares V6 T(p) for March 1979 at 38°N with that from the temperature climatology at 40°N from Barnett and Corney (or BC, 1985). Those (V6 – BC) temperature values include a five-point running average of the SPARC-DI V6 monthly T(p) profile above the 30-hPa level to account for the broader vertical weighting functions of the satellite measurements of BC. The difference profiles, V6-BC, have values no greater than the bias estimates for T(p) (in row 2) at most pressure altitudes.

157

Figure 3 shows V6 zonal average H₂O for March 1979 from SPARC-DI. H₂O is effectively a tracer of the mean meridional circulation, which moves upward from the tropical tropopause to the middle stratosphere and then poleward toward higher latitudes. Minimum values of H₂O are of order 3.5 ppmv in the tropics between 50 and 70 hPa. The sharply increasing H₂O near the



162 tropical tropopause is due, in part, to residual emissions from cirrus cloud tops that were not
 163 screened completely from the bottom of the LIMS H₂O radiance profiles prior to retrieval.
 164 Highest values of H₂O are at upper altitudes (> 6.0 ppmv) and are due to the oxidation of
 165 methane (CH₄) to H₂O, followed by its net transport and accumulation at higher latitudes. NLTE
 166 processes also cause enhancements of H₂O radiance near the stratopause during daytime. Those
 167 uncorrected NLTE effects extend downward to lower altitudes for retrieved V6 H₂O, although
 168 the effects are small for the middle and lower stratosphere (Mertens et al., 2002). Estimates of
 169 the effect of temperature bias for V6 H₂O are in Table 1 (row 4) from Remsberg et al. (2009).

170

171 **3 Measurement, retrieval, and day/night differences for temperature**

172 Nimbus 7 was in a near-polar orbit, and LIMS made measurements at ~1 pm local time along its
 173 ascending (A or south-to-north traveling) orbital segments and at ~11 pm for its descending (D
 174 or north-to-south traveling) segments. The A-D time difference is of the order of 10 hours
 175 because LIMS viewed the atmosphere 146.5° clockwise of the spacecraft velocity vector or 33.5°
 176 counterclockwise from its negative velocity vector, as seen from overhead. In other words,
 177 LIMS viewed atmospheric tangent layers in opposing meridional directions for the NH and
 178 through the tropics or toward the SSE along A segments and toward the NNW along D segments
 179 (Gille and Russell, 1984). The A and D view paths for middle latitudes of the SH are more
 180 nearly in a zonal direction and toward the NNW, respectively, due to the orbital inclination of
 181 Nimbus 7.

182

183 Figure 4 shows V6 A-D temperatures March. The differences in the upper stratosphere indicate
 184 how well the effects of the temperature tides have been resolved (Remsberg et al., 2004).
 185 Tropical differences are due mainly to diurnal tides, and they become large in the mesosphere.
 186 Tidal amplitudes for the tropics increase with altitude in Fig. 4, ranging from -2 K at 15 hPa to
 187 +4 K at 1.5 hPa. Those V6 tidal variations agree qualitatively with ones from rocket Datasonde
 188 profiles (Hitchman and Leovy, 1985; Finger et al., 1975). Fig. 4 also shows the expected 180°
 189 change of phase for A-D T(p) from the tropics to subtropics. Accurate determinations of T(p)
 190 versus latitude depend critically on knowledge of the Nimbus 7 spacecraft attitude. That



191 information for a complete orbit comes empirically from profiles of calculated-to-measured
 192 radiance ratios for the LIMS narrow CO₂ channel and can lead to a bias error for A-D T(p). Any
 193 bias in the orbital attitude will affect T(p) at all altitudes; that error source is small according to
 194 the good comparisons of the LIMS-derived geopotential heights versus those from operational
 195 analyses at both the 10-hPa and 46-hPa levels (Remsberg et al., 2004). Even so, Fig. 4 also
 196 shows that there are residual A-D T(p) differences at 70 hPa that are opposite in sign at 40°S and
 197 30°N, or just where there are large, opposing meridional gradients in T(p) in Fig. 2.

198

199 The measured ozone radiance profiles contain the full effects of any atmospheric variations in
 200 T(p). As an example, Figure 5 shows zonal mean, ozone radiance differences (A-D) for one day
 201 (March 15). Radiance differences in the tropics have a change in sign from positive at 3 hPa to
 202 negative in the lower mesosphere, and they correspond directly with A-D changes in temperature
 203 in Fig. 4. Positive A-D radiances at middle latitudes of the lower mesosphere are due to the
 204 dominance of NLTE daytime radiances from CO₂ and O₃, as compared with the tidal effects
 205 from T(p).

206

207 There are negative A-D ozone radiances of up to -5% in the stratosphere at the northern middle
 208 latitudes, and they are a result of the meridional decrease of T(p) (in Fig. 2) from the northern
 209 subtropics toward higher latitudes. More of the measured radiance in that region comes from the
 210 front end of the tangent layer or from the colder side on the A orbital segment and from the
 211 warmer side on the D segment, leading to negative A-D radiances. The LIMS algorithms for
 212 temperature and species account for horizontal temperature gradients, to first order (Roewe et al.,
 213 1982; Gille et al., 1984; Remsberg et al., 2004 and 2007). T(p) gradients for V6 are from daily
 214 surface maps from the average (A+D) V5 temperature fields, where the meridional resolution of
 215 the V5 fields is no better than half that of V6, or 4° versus 2° of latitude. Those average (A+D)
 216 T(p) gradients from V5 underestimate the true atmospheric gradients and result in slight biases
 217 between the A and D T(p) values at the same latitude. Kiefer et al. (2010) analyzed for effects of
 218 a T(p) gradient in more detail using data from the limb-infrared, Michelson Interferometer for
 219 Passive Atmospheric Sounding (MIPAS) experiment. They confirm that it is important to



correct for $T(p)$ gradients in the respective A and D views for accurate retrievals of species from their corresponding A or D radiance profiles.

V6 retrievals of $T(p)$ employ a starting reference pressure level P_0 near 20 hPa (~26 km relative altitude) and hydrostatic conversions to pressure-altitude that extend both upward and downward from P_0 . The algorithm makes forward radiance calculations for the two broadband CO_2 channels and compares them with their measured radiance profiles. $T(p)$ differences (A-D) of the same sign will impart growing A-D radiance versus pressure differences away from P_0 . Both P_0 and $T(p)$ undergo iteration until the calculated and measured, tangent layer radiances agree to within the noise levels of the measured radiances over the pressure range of 2 to 20 hPa. Yet, the noise value for the narrow CO_2 channel is nearly 2% of the signal at 2 hPa. This level is where the diurnal temperature tide has a larger amplitude and can impart a systematic, A-D bias in P_0 . An A-D bias error in radiance is also significant; a calibration error of 1% causes a 0.6 K error in $T(p)$ for the middle and upper stratosphere (Remsberg et al., 2004, Table 3). Another possible source of (A-D) bias for $T(p)$ can arise from a residual uncertainty of the viewing attitude of LIMS along an orbit, its empirical “twist factor”.

Roewe et al. (1982) showed that adjustments for horizontal gradients in $T(p)$ affect species retrievals from calculations of the Planck blackbody radiance throughout the stratosphere, as well as the registration of their radiance versus pressure profiles, mainly in the lower stratosphere. The region of negative, A-D ozone channel radiance in Fig. 5 has values that increase toward the lower stratosphere because of persistent A-D $T(p)$ biases plus the hydrostatic registration of the measured radiance profiles with pressure-altitude. The radiance differences are negative at middle latitudes of the NH but positive in the SH. Ozone radiance at 10 hPa (not shown) increases from 40°N to 18°N, holds nearly steady in the tropics, and decreases from 20°S to 40°S, mainly due to the changing ozone with latitude (Fig. 1). Gordley and Russell (1981) showed that the bulk of the LIMS broadband ozone radiance for the middle and lower stratosphere also comes from the near side of the tangent layer (displaced toward the satellite by about 300 to 500 km or ~3° to 6° of latitude). Such tangent layer asymmetries explain part of the observed change of sign of the A-D radiances between the two hemispheres in Fig. 5.



250 Nevertheless, the mass path algorithm of the V6 forward model simulates radiance along a well-
 251 resolved limb path, using rigorous ray tracing methods, including refraction effects and first-
 252 order corrections for temperature gradients, and assigns an observed tangent altitude
 253 corresponding to the center of the measurement field-of-view.

254

255 Roewe et al. (1982) showed that adjustments for the path gradients of the ozone mixing ratio
 256 itself imparts only small A-D mixing ratio differences (~2%). Thus, the V6 retrievals do not
 257 account for species gradients. The V6 algorithms are no longer operational for further studies of
 258 the effects of T(p) gradients on ozone and H₂O. Instead, in the next section we present
 259 diagnostic plots based on the V6 Level 3 data themselves to indicate that there are residual biases
 260 in the distributions of V6 T(p) and that they carry over to V6 ozone and H₂O.

261

262 **4 Day/night differences in V6 ozone and water vapor**

263 *4.1 Upper stratosphere*

264 Remsberg et al. (1984; 2007) reported on the occurrence of day/night, or the A-D ozone values;
 265 those results are similar for V5 and V6. Figure 6 shows the distribution of V6 A-D ozone for
 266 March as divided by the zonal mean ozone, such that the pattern of systematic differences is a
 267 percentage of the zonal average ozone. Photochemical calculations by Haigh and Pyle (1982)
 268 predict about a -2% change in ozone for a +1 K change in T(p) at 1.5 hPa. The V6 tropical
 269 ozone differences in Fig. 6 grow to nearly -3% near 1 hPa and are opposite in sign to the
 270 temperature tides of Fig. 4. Thus, the V6 ozone of the tropical upper stratosphere agrees
 271 reasonably with effects from the observed temperature tides.

272

273 Sakazaki et al. (2013, their Fig. 4) also reported diurnal model calculations of tropical day-night
 274 ozone values of -3.5% at 44 km (~1.7 hPa) at the local times of the LIMS observations; their
 275 microwave observations of ozone agree with them. They also obtained A-D ozone variations of
 276 +3.5% at 34 km (~6 hPa) from the photochemistry of odd oxygen during daytime, and those
 277 differences decay away from the Equator. Yet, the V6 A-D tropical ozone differences are nearly



twice as large at 6 hPa in Fig. 6, and they disagree with modeled changes in Frith et al. (2020). There are also separate, rather large V6 ozone differences at middle latitudes of the upper stratosphere, where effects from temperature tides are small. The rather large A-D ozone values (~4 to 6%) at SH middle latitudes correspond to where the A-D ozone radiances in Fig. 5 are increasing with altitude by +2 to +4% and where A-D T(p) is weakly negative. While these results are consistent with the effects of temperature on retrieved ozone through the V6 algorithm, the ozone radiances may also have an A-D pressure registration bias due to the persistently, negative A-D T(p) in that region. The axis of the positive A-D ozone anomaly at NH middle latitudes in Fig. 6 overlays the region of rather large, meridional T(p) gradients in Fig. 2.

Figures 7 and 8 provide supporting evidence that uncorrected, residual temperature gradients are a likely cause of the A-D ozone anomalies in Fig. 6. Fig. 7 shows zonal (wave) standard deviations (SD) about the zonal average of the combined (A+D) temperature fields for March, where the SD values are from the LIMS SPARC-DI data product. There is significant zonal wave activity at middle to high latitudes in both the NH and SH, and one must account for their separate A and D horizontal gradients for accurate ozone retrievals. Fig. 8 is the corresponding, zonal wave standard deviations for ozone that have a maximum value of 0.40 ppmv near 65°N and 1 hPa, or where transport affects ozone as well as chemistry.

The V6 H₂O retrievals are more sensitive than ozone to biases in T(p) at 3 hPa (in Table 1) because most of the V6 H₂O radiance comes from its strong, nearly saturated lines. Figure 9 shows the H₂O A-D mixing ratio values for March. Both species are altered by horizontal gradients in T(p) in the same way in calculations of their Planck radiances. The locus of maximum percentage difference for H₂O in the SH differs from that of ozone (Fig. 6) in the middle to upper stratosphere because their respective mixing ratios also have gradients that differ. The effect of the tropical temperature tide on H₂O is not apparent at 1.5 hPa because of the excess of NLTE radiances of H₂O at and above that level during daytime.



307 *4.2 Middle and lower stratosphere*

308 V6 A-D ozone mixing ratio in Fig. 6 is near zero at 20 hPa. This feature occurs where V6 A-D
 309 for $T(p)$ in Fig. 4 is also small, or where there is iteration of P_0 and from which a hydrostatic
 310 integration occurs both above and below that level. The ozone differences become negative
 311 below that level across the tropics and in the NH, where the vertical gradient of ozone (Fig. 2) is
 312 large and subject to small A-D differences in the registration of the ozone radiance profiles.
 313 However, the ozone differences at SH middle latitudes remain positive down to the 100-hPa
 314 level; only tangent views along the descending orbital path are in a nearly meridional direction at
 315 those latitudes. In particular, the A-D ozone values in Fig. 6 are rather large at 40°S and 30°N
 316 (40 to 100 hPa), and they are opposite in sign to the A-D $T(p)$ differences of order ± 1 K in Fig. 4.
 317 This finding agrees with the estimates of $T(p)$ effects at 50 hPa in Table 1, where a bias of -1.3 K
 318 leads to a +20% bias in ozone. The A-D temperature biases are large just where the meridional
 319 temperature gradients are also large (Fig. 2) and corrections for them are too small.

320

321 A-D values for H_2O in Fig. 9 have an opposite character from those of ozone from 50 to 100 hPa
 322 because the vertical gradient of H_2O in Fig. 3 is also opposite that of ozone in the lowermost
 323 stratosphere. This finding is a clear indication of how the same A-D $T(p)$ biases can affect
 324 retrieved ozone and H_2O differently. The few correlative balloon measurements of H_2O during
 325 1978/1979 are too uncertain to judge whether the V6 A or D H_2O profiles are more accurate.

326

327 One particular feature is that both A-D ozone and H_2O are positive and approach 8% at about 10
 328 hPa and 25°N. The SD values for temperature and ozone show local increases there, too. Fig.
 329 10 gives details of the NH distribution of V6 ozone on the 10-hPa surface for one day, March 15,
 330 for a gridding (at 2° lat; 5.625° long) from its 13 zonal Fourier coefficients (a zonal mean and 6
 331 cosine and sine values) of the Level 3 product (Remsburg and Lingenfelter, 2010). There is a
 332 meridional gradient in the ozone field at the equatorward edge ($\sim 25^\circ$ N) of a much larger mid
 333 latitude region of near zero gradient—a result of the effects of the efficient mixing of air from
 334 higher latitudes during late winter. Zonal average, A-D temperatures at 10 hPa in Fig. 4 are of
 335 order -1 K at 15°N but then change to weakly positive at 25°N. The corresponding NH field of



336 T(p) on March 15 is in Fig. 11, and it shows a narrow belt of slightly higher temperature near
 337 25°N, or just where the A-D meridional gradient of T(p) changes sign in Fig. 4. Such small T(p)
 338 differences also affect the registration of the ozone and H₂O radiance profiles. There are
 339 unexpected, tropical A-D ozone mixing ratios of order 5% at 10 hPa for all the LIMS months.
 340 Those anomalies appear to migrate across the tropics and subtropics with the season, perhaps
 341 indicating that the residual biases in the T(p) distributions are related to seasonal changes for the
 342 Brewer-Dobson circulation (see temperature and ozone results for other selected months in the
 343 *Supplemental Material*).

344

345 LIMS HNO₃ is optically thin and its retrievals are much less sensitive to temperature bias via the
 346 Blackbody function (Table 1, row 5). Its radiance profile measurements also come more nearly
 347 from the center of the tangent layer, unlike those of ozone and water vapor. Maximum mixing
 348 ratios for HNO₃ occur at about 20 hPa in the tropics and 30 hPa at high latitudes (e.g., as in Fig. 1
 349 of Remsberg et al., 2010) or similar to those of ozone. Figure 12 is a plot of A-D for V6 HNO₃
 350 (in %) for March for comparison with that of ozone in Fig. 6, and there are two important
 351 differences between them. First, A-D for HNO₃ is uniformly negative in the middle to upper
 352 stratosphere from photolysis during daytime, whereas A-D for ozone is slightly positive from
 353 enhanced production during the day. Secondly, there are no apparent variations in A-D for
 354 HNO₃ in the upper stratosphere at 40°S or near 10 hPa at 25°N from effects of co-located,
 355 horizontal temperature gradients. Yet, the patterns with latitude of A-D are very similar for both
 356 HNO₃ and ozone in the lower stratosphere and indicate the effects of A-D temperatures on the
 357 registration of the radiance profiles, prior to their retrievals to mixing ratios.

358

359 **5 Ozone comparisons with rocket-borne measurements**

360 This section considers the quality of the V6 ascending (daytime) ozone of the middle and upper
 361 stratosphere at NH middle latitudes; there is only one corresponding comparison for the
 362 descending (nighttime) ozone (not shown, but see Fig. 13 of Remsberg et al., 1984). Krueger
 363 (1973) developed meteorological rocket-borne, UV-absorption ozonesonde (ROCOZ)
 364 instruments in the 1960s and 1970s and made routine soundings of middle atmosphere ozone.



365 To measure absorption of sunlight in three altitude regions between 15 and 60 km, ROCOZ used
 366 four interference filters procured commercially in batches for uniformity. There were launches
 367 of ROCOZ instruments for the validation of LIMS (seven flights) and of SBUV ozone at low-
 368 (Natal, Brazil), mid- (Wallops Island, VA) and high- (Fort Churchill and Primrose Lake,
 369 Canada) latitudes. Remsberg et al. (1984) reported on comparisons of the V5 ozone with
 370 ROCOZ soundings and found mean differences (V5 minus ROCOZ) that varied from 5% in the
 371 upper stratosphere to 16% in the lower stratosphere. The RMS differences were rather large
 372 though (12% to 23%, respectively), and there were concerns about the stability of the batch of
 373 UV interference filters used in the ROCOZ instruments from late 1978 through mid-1979.

374

375 An early ‘ozone climatology’ was produced from the greater than 200 ROCOZ soundings
 376 launched between 1965 and 1990 at rocket ranges from the equator to high latitudes of both
 377 hemispheres (Krueger, 1984; WOUDC). The ROCOZ flights include a SH latitude survey,
 378 calibration flights for the Orbital Geophysical Observatory (OGO-4) UV spectrometer (London
 379 et al., 1977), low latitude baseline flights from Antigua, high latitude flights from Fort Churchill
 380 and Primrose Lake, validation flights for the Backscatter Ultraviolet (BUV) experiment on
 381 Nimbus 4, and a regular monthly series of measurements from Wallops Island, VA. In fact, the
 382 1976 U.S. Standard Atmosphere mid-latitude ozone model makes use of rocket data from seven
 383 international experimenters, including ROCOZ (Krueger and Minzner, 1976).

384

385 Krueger (1984) also compiled separate monthly averages of soundings from Wallops Island
 386 (38°N) during the period of March 1976 through September 1978. Uncertainty about the UV
 387 filters was not at issue for those soundings. As an example, Fig. 13 compares the April average
 388 from ROCOZ with the monthly zonal mean V6 Level 3 daytime ozone at 38°N for April 1979,
 389 when wave activity and zonal variations about the V6 daily zonal means are <3%. Even though
 390 the V6 profiles contain 18 values per decade of pressure (spaced ~0.88 km), we plot only every
 391 other point because the V6 data carry an effective vertical resolution of ~3.7 km. The horizontal
 392 bars at 0.3, 1, 2, and 10 hPa represent estimates of bias error for V6 ozone from Remsberg et al.
 393 (2007, their Table 1). The ROCOZ profiles are averages of the three April soundings for 1976-
 394 1978, and the horizontal bars at 0.5, 1.5, 3, 7, and 15 hPa are their estimated uncertainty of <10%



395 (or $<7\%$ for ozone number density versus altitude, plus $<3\%$ for the conversion to mixing ratio
 396 versus pressure, as taken from Table II-7 of Krueger (1984)). Fig. 13 indicates agreement to
 397 within the estimates of bias error for V6 ozone at most altitudes of the stratosphere. V6 ozone is
 398 higher than ROCOZ ozone from ~ 2.0 to 0.3 hPa.

399

400 Figure 14 shows V6 daytime minus ROCOZ average profiles at Wallops Island (38°N) for
 401 November, March, April, and May. The ozone differences are within their combined error
 402 estimates for the middle stratosphere but are larger in the upper stratosphere and, especially, the
 403 mesosphere. The increasingly positive, V6 day minus ROCOZ differences from winter to late
 404 spring in the lower mesosphere are due to uncorrected NLTE emissions from CO_2 and ozone that
 405 increase toward lower solar zenith angles (Edwards et al., 1996; Manuilova et al., 1998). On the
 406 other hand, the V6 daytime ozone of April and May is also larger than ROCOZ ozone in the
 407 uppermost stratosphere, where NLTE should not be an issue. This finding implies that there may
 408 be a slight negative bias for V6 T(p) at those high altitudes (see Table 1). Another possibility is
 409 that the limited ROCOZ climatology at Wallops Islands may not be truly representative of zonal
 410 average ozone for those months of 1979. In the next section, we report on time series of fields of
 411 potential vorticity, ozone, and H_2O from their Level 3 combined (A+D) products for the middle
 412 stratosphere, where those parameters are not expected to have diurnal variations and should serve
 413 as tracers of atmospheric transport.

414

415 **6 Seasonal transport of V6 ozone and water vapor**

416 Dunkerton and DeLisi (1986) made use of LIMS V5 GPH and temperature data to calculate
 417 potential vorticity (PV) and then to show how PV evolved in the NH on the 850 K potential
 418 temperature (~ 10 hPa) surface during January and February 1979. Butchart and Remsberg (BR,
 419 1986) also calculated PV from the V5 data and plotted its evolution during the winter of 1978-
 420 1979 in terms of the fractional area of the NH enclosed by the horizontal projection of a given
 421 PV contour on the 850 K surface. These so-called, area diagnostic analyses of BR work well for
 422 a parameter like PV that is monotonic with latitude, having its highest value at the Pole.

423



424 New time series analyses of PV from the combined V6 data are in Fig. 15, calculated from the
 425 Level 3, daily 6-wavenumber, zonal coefficients of GPH and temperature. Equivalent latitude
 426 (on the right ordinate) represents the latitude at which a zonally symmetric PV contour would lie
 427 if it enclosed the given fractional area shown on the left ordinate. PV data for Fig. 15 have a 7-
 428 day smoothing, and the NH fractional area extends only to 20° equivalent latitude, since
 429 calculations of absolute vorticity are not so accurate for latitudes near the Equator. The PV
 430 results for V6 are nearly identical to those for V5 in BR (their Fig. 4). Notably, the polar vortex
 431 (defined by highest PV values) erodes during winter and the adjacent ‘surf-zone’, having much
 432 lower PV gradients, expands in area due to the ‘breaking’ of planetary waves and the associated
 433 meridional mixing of vortex and lower latitude air.

434

435 Ozone is an effective tracer of the transport of air in and around the winter polar vortex on the
 436 850 K surface (~10 hPa) (Leovy et al., 1985). Ozone also varies nearly monotonically at this
 437 level, but with highest values at low latitudes and lowest values near the Pole. BR analyzed the
 438 evolution of V5 ozone (see their Fig. 10b). They compared its changes with those of PV and
 439 found good correspondence for the large-scale features of the two distributions. Fig. 16 is the
 440 new ozone time series at 850 K from the gridded V6 data, and it compares well with the
 441 calculations of BR from the V5 ozone. One significant change with V6 is that the ozone
 442 contours of 6.8 through 7.2 ppmv of early February indicate very weak gradients within the surf
 443 zone, as it expands following the major warming event of late January. There is also an
 444 associated, diabatic cross-isentropic transport of ozone within the surf zone during that time
 445 (e.g., Butchart, 1987). The improved continuity of the ozone time series from V6 is a result of
 446 the better spatial sampling for the radiances, of the retrievals of T(p) profiles, and of the
 447 corresponding changes for the registration of the ozone radiances and retrieved ozone mixing
 448 ratio profiles.

449

450 Water vapor is also a tracer of the net transport in the middle stratosphere. Figure 17 shows the
 451 corresponding time series of V6 H₂O at 850 K. The V6 H₂O mixing ratio contours vary more
 452 smoothly than those from the V5 data in BR (their Fig. 12); the retrieved V6 H₂O profiles are
 453 better resolved spatially and have better precision. There is good correspondence between H₂O,



PV, and ozone for the location and evolution of the edge of the polar winter vortex and for the expansion of the region of weak gradients at middle latitudes. Low values of H₂O extend to the northern middle latitudes and high values of H₂O descend within the polar vortex from November through January, indicating an acceleration of the Brewer/Dobson circulation during that winter. There is also a modest expansion of weak H₂O gradients between 40°N to 60°N equivalent latitude from mid-November to mid-December. This region coincides with the time of the Canadian warming and an exchange of air between polar and middle latitudes.

461

7 Summary and recommendations

This study provides some insight about the quality of the LIMS V6 Level 3 product and about the generation of daily gridded ozone and H₂O distributions on pressure surfaces. Monthly zonal mean distributions are available within the SPARC-DI database for comparisons with model simulations of middle atmosphere ozone. We also provide the corresponding monthly zonal mean distributions of temperature for SPARC-DI and diagnostic evidence of effects of residual temperature biases in the V6 ozone and H₂O distributions. Both species exhibit small, ascending minus descending (A-D or day minus night at most latitudes) anomalies, especially in the middle and lower stratosphere. A-D ozone and H₂O values are larger than expected due to not accounting for all of the horizontal temperature structure, which affects forward radiance calculations through the Planck blackbody function, the retrievals of T(p), and the registration of the species radiance profiles with pressure. It may be that the V6 species distributions within the SH have better accuracy from along its ascending (A) orbital segments, since the tangent view paths for its profiles are more nearly in a zonal direction and do not have significant T(p) gradients.

477

Remsberg et al. (2013) reported that an assimilation of SBUV ozone along with the V6 A and D Level 2 ozone profiles provides ozone distributions that agree well with balloon-sonde ozone in the lower stratosphere. Yet, we do not recommend assimilation studies based on only the V6 ozone profiles because of their small, but persistent A-D differences, particularly at the edge of and within the winter polar vortex (Krzysztof Wargan, private communication, 2017). The V6



483 H₂O profiles will present similar assimilation problems. Instead, we recommend that researchers
484 make use of the average (A+D) V6 Level 3 product and/or the SPARC-DI monthly, zonal
485 average distributions for science studies of both stratospheric ozone and H₂O wherever diurnal
486 variations are not expected. Tegtmeier et al. (2013) compared the combined V6 monthly
487 stratospheric ozone distributions with ones from other satellite-based limb sensors, and they
488 found good agreement. Thereafter, Shepherd et al. (2014) integrated the SPARC-DI V6 monthly
489 zonal mean ozone above the tropopause and subtracted it from observed total ozone as part of
490 their assessment of long-term trends of tropospheric ozone from models for 1978 and onward.

491

492 Remsberg et al. (2007, their Fig. 8b) found that zonal average V6 ozone in the middle
493 stratosphere is higher than SBUV ozone by 4%, which is well within the combined systematic
494 errors of both experimental datasets. Correlative ozone measurements for the middle to upper
495 stratosphere are too few and too inaccurate in 1978/1979 to determine whether the V6 A or D
496 ozone is more accurate. Thus, we considered V6 monthly profile data versus a monthly daytime
497 ozone climatology of the late 1970s obtained with the rocket-borne, uv-absorption (ROCOZ)
498 technique at Wallops Island, VA. We found agreement within their respective errors, except for
499 the uppermost stratosphere and the lower mesosphere. We also calculated time series of V6
500 Level 3 ozone and H₂O at 850 K and looked for consistency between their fields and those of
501 PV. In general, we found good agreement with similar studies of BR (1986) that use the V5
502 dataset. However, the V6 time series show better continuity during dynamically active periods.

503

504 The LIMS experience has been of benefit for the design of follow-on broadband, limb infrared
505 measurements. One satellite experiment, the Sounding of the Atmosphere using Broadband
506 Emission Radiometry (SABER), has been obtaining measurements of temperature, ozone, and
507 H₂O from 2002-2020 (e.g., Remsberg et al., 2008; Rong et al., 2009). Improvements of SABER
508 over LIMS include: (1) reductions in electronics and detector noise for its narrow-band and
509 wide-band CO₂ channels by factors of 5 and 16, respectively, and for its ozone channel by a
510 factor of 20; (2) common, 2-km IFOVs for its CO₂ (for temperature) and species channels to
511 account for diurnal temperature signals in the retrievals of ozone and H₂O; (3) an ozone filter
512 bandpass of about 1000 to 1150 cm⁻¹ to avoid the NLTE emissions from the CO₂ laser band at



513 960 cm⁻¹; and (4) NLTE algorithms for retrievals of T(p), ozone, and H₂O in the mesosphere.
 514 SABER orbital attitude information is accurate. Its tangent view paths are 90° away from the
 515 spacecraft velocity vector or in nearly a zonal direction for the low and middle latitudes, where
 516 temperature gradients are weak. There is little need to correct for T(p) gradients in the SABER
 517 algorithms, except when viewing the high latitudes. Accordingly, the diurnal temperature and
 518 ozone variations from SABER compare reasonably with those from microwave measurements
 519 and with model estimates (e.g., Huang et al., 2010a and 2010b; Frith et al., 2020).

520

521 **Data Availability**

522 The LIMS V6 data archive is at the NASA EARTHDATA site of EOSDIS and its website:
 523 <https://search.earthdata.nasa.gov/search?q=LIMS>). The ROCOZ ozone climatology at Wallops
 524 Island is available from co-author, Arlin Krueger, upon request. The SPARC-Data Initiative site
 525 is located at <https://www.sparc-climate.org/data-centre/data-access/sparc-data-initiative/>. We
 526 acknowledge the individual instrument teams and respective space agencies for making their
 527 measurements available, and the Data Initiative of WCRP's (World Climate Research
 528 Programme) SPARC (Stratospheric Processes and their Role in Climate) project for organizing
 529 and coordinating the compilation of the chemical trace gas datasets used in this work.

530

531 *Author Contributions.* ER prepared most of the figures and wrote the manuscript with
 532 contributions from all co-authors. MN produced plots of the ascending minus descending
 533 radiances. VLH prepared the time series plots of PV, ozone, and H₂O. AK provided his
 534 rocketsonde data on ozone and temperature and their estimated errors.

535

536 *Acknowledgements.* The authors are grateful to John Burton, L. L. Gordley, B. T. Marshall, and
 537 R. E. Thompson for producing the V6 Level 2 dataset. Gretchen Lingenfelter generated the V6
 538 Level 3 zonal Fourier coefficient data. We thank John Gille and Ernest Hilsenrath, who read and
 539 commented on a draft version of the manuscript. VLH acknowledges support from NSF
 540 CEDAR grant 1343031, NASA LWS grant NNX14AH54G, NASA HGI grant NNX17AB80G,
 541 and from NASA HSR grant 80NSSC18K1046. EER and MN carried out their work while
 542 serving as a Distinguished Research Associates of the Science Directorate at NASA Langley.



543 **References**

- 544 Barnett, J., and Corney, M.: Middle atmosphere reference model derived from satellite data, in
 545 Handbook for Middle Atmosphere Program, Labitzke, K, Barnett, J. J., and Edwards, B., (Eds.),
 546 vol. 16, 47-137, NASA Contractor Report 176321, Document ID 19860003346,
 547 <https://ntrs.nasa.gov>, (last access November 12, 2019), 1985.
- 548
- 549 Butchart, N.: Evidence for planetary wave breaking from satellite data: the relative roles of
 550 diabatic effects and irreversible mixing, in *Transport Processes in the Middle Atmosphere*,
 551 Visconti, G., and Garcia, R. (Eds.), D. Reidel Publishing Co., Dordrecht, Holland, pp. 121-136,
 552 1987.
- 553
- 554 Butchart, N. and Remsberg, E. E.: The area of the stratospheric polar vortex as a diagnostic for
 555 tracer transport on an isentropic surface, *J. Atmos. Sci.*, 43, 1319-1339,
 556 [https://doi.org/10.1175/1520-0469\(1986\)043%3C1319:TAOTSP%3E2.0.CO;2](https://doi.org/10.1175/1520-0469(1986)043%3C1319:TAOTSP%3E2.0.CO;2), 1986.
- 557
- 558 Dunkerton, T. J. and DeLisi, D. P.: Evolution of potential vorticity in the winter stratosphere of
 559 January-February 1979, *J. Geophys. Res.* 91, 1199-1208,
 560 <https://doi.org/10.1029/JD091iD01p01199>, 1986.
- 561
- 562 Edwards, D. P., Kumer, J. B., Lopez-Puertas, M., Mlynczak, M. G., Gopalan, A., Gille, J. C., and
 563 Roche, A.: Non-local thermodynamic equilibrium limb radiance near 10 μm as measured by
 564 UARS CLAES, *J. Geophys. Res.*, 101, D21, 26,577-26,588, <https://doi.org/10.1029/96JD02133>,
 565 1996.
- 566
- 567 Finger, F. G., Gelman, M. E., Schmidlin, F. J., Leviton, R., and Kennedy, V. W.: Compatibility
 568 of meteorological rocketsonde data as indicated by international comparisons tests, *J. Atmos.*



- 569 Sci., 32, 1705-1714, [https://doi.org/10.1175/1520-](https://doi.org/10.1175/1520-0469(1975)032%3C1705:COMRDA%3E2.0.CO;2)
 570 [0469\(1975\)032%3C1705:COMRDA%3E2.0.CO;2](https://doi.org/10.1175/1520-0469(1975)032%3C1705:COMRDA%3E2.0.CO;2), 1975.
- 571
- 572 Frith, S. M., Bhartia, P. K., Oman, L. D., Kramarova, N. A., McPeters, R. D., and Labow, G. J.:
 573 Model-based climatology of diurnal variability in stratospheric ozone as a data analysis tool,
 574 Atmos. Meas. Tech., 13, 2733-2749, <https://doi.org/10.5194/amt-13-2733-2020>, 2020.
- 575
- 576 Gille, J. C. and Russell III, J. M.: The limb infrared monitor of the stratosphere: experiment
 577 description, performance, and results, J. Geophys. Res., 84, 5125-5140,
 578 <https://doi.org/10.1029/JD089iD04p05125>, 1984.
- 579
- 580 Gille, J. C., Russell III, J. M., Bailey, P. L., Gordley, L. L., Remsberg, E. E., Lienesch, J. H.,
 581 Planet, W. G., House, F. B., Lyjak, L. V., and Beck, S. A.: Validation of temperature retrievals
 582 obtained by the limb infrared monitor of the stratosphere (LIMS) experiment on NIMBUS 7, J.
 583 Geophys. Res., 89, 5147-5160, <https://doi.org/10.1029/JD089iD04p05147>, 1984.
- 584
- 585 Gordley, L. L. and Russell, J. M.: Rapid inversion of limb radiance data using an emissivity
 586 growth approximation, Appl. Opt., 20, 807-813, <https://doi.org/10.1364/AO.20.000807>, 1981.
- 587
- 588 Haigh, J. D., and Pyle, J. A.: Ozone perturbation experiments in a two-dimensional circulation
 589 model, Q. J. Roy. Meteorol. Soc., 108, 551-574, <https://doi.org/10.1002/qj.49710845705>, 1982.
- 590
- 591 Hitchman, M. H., and Leovy, C. B.: Diurnal tide in the equatorial middle atmosphere as seen in
 592 LIMS temperatures, J. Atmos. Sci., 42, 557-561, [https://doi.org/10.1175/1520-](https://doi.org/10.1175/1520-0469(1985)042%3C0557:DTITEM%3E2.0.CO;2)
 593 [0469\(1985\)042%3C0557:DTITEM%3E2.0.CO;2](https://doi.org/10.1175/1520-0469(1985)042%3C0557:DTITEM%3E2.0.CO;2), 1985.
- 594



- 595 Huang, F. T., McPeters, R. D., Bhartia, P. K., Mayr, H. G., Frith, S. M., Russell III, J. M., and
 596 Mlynczak, M. G.: Temperature diurnal variations (migrating tides) in the stratosphere and lower
 597 mesosphere based on measurements from SABER on TIMED, *J. Geophys. Res.*, 115, D16121,
 598 <https://doi.org/10.1029/2009JD013698>, 2010a.
- 599
- 600 Huang, F. T., Mayr, H. G., Russell III, J. M., and Mlynczak, M. G.: Ozone diurnal variations in
 601 the stratosphere and mesosphere, based on measurements from SABER on TIMED, *J. Geophys.*
 602 *Res.*, 115, D24308, <https://doi.org/10.1029/2010JD014484>, 2010b.
- 603
- 604 Kiefer, M., Arnone, E., Dudhia, A., Carlotti, M., Castelli, E., von Clarmann, T., Dinelli, B. M.,
 605 Kleinert, A., Linden, A., Milz, M., Papandrea, E., and Stiller, G.: Impact of temperature field
 606 inhomogeneities on the retrieval of atmospheric species from MIPAS IR limb emission spectra,
 607 *Atmos. Meas. Tech.*, 3, 1487–1507, <https://doi.org/10.5194/amt-3-1487-2010>, 2010.
- 608
- 609 Krueger, A. J.: The mean ozone distribution from several series of rocket soundings to 52 km at
 610 latitudes from 58°S to 64°N, *PAGEOPH*, 106, 1272-1280, <https://doi.org/10.1007/BF00881079>,
 611 1973.
- 612
- 613 Krueger, A. J: Inference of photochemical trace gas variations from direct measurements of
 614 ozone in the middle atmosphere, Doctoral Dissertation, Colorado State Univ., Fort Collins, CO,
 615 1984, (available for download from ResearchGate:
 616 [https://www.researchgate.net/publication/253654486_Inference_of_photochemical_trace_gas_va](https://www.researchgate.net/publication/253654486_Inference_of_photochemical_trace_gas_variations_from_direct_measurements_of_ozone_in_the_middle_atmosphere)
 617 [riations_from_direct_measurements_of_ozone_in_the_middle_atmosphere](https://www.researchgate.net/publication/253654486_Inference_of_photochemical_trace_gas_variations_from_direct_measurements_of_ozone_in_the_middle_atmosphere)).
- 618
- 619 Krueger, A. J. and Minzner, R. A.: A mid-latitude ozone model for the 1976 U. S. standard
 620 atmosphere, *J. Geophys. Res.*, 81, 4477-4481, <https://doi.org/10.1029/JC081i024p04477>,
 621 1976.
- 622



- 623 Leovy, C. B., Sun, C-R., Hitchman, M. H., Remsberg, E. E., Russell, III, J. M., Gordley, L. L.,
 624 Gille, J. C., and Lyjak, L. V.: Transport of ozone in the middle stratosphere: evidence for
 625 planetary wave breaking, *J. Atmos. Sci.*, 42, 230-244, [https://doi.org/10.1175/1520-](https://doi.org/10.1175/1520-0469(1985)042%3C0230:TOOITM%3E2.0.CO;2)
 626 [0469\(1985\)042%3C0230:TOOITM%3E2.0.CO;2](https://doi.org/10.1175/1520-0469(1985)042%3C0230:TOOITM%3E2.0.CO;2), 1985.
- 627
- 628 London, J., Frederick, J. E., and Anderson, G. P.: Satellite observations of the global distribution
 629 of stratospheric ozone, *J. Geophys. Res.*, 82, 2543-2556,
 630 <https://doi.org/10.1029/JC082i018p02543>, 1977.
- 631
- 632 Lopez-Puertas, M. and Taylor, F. W.: Non-LTE Radiative transfer in the Atmosphere, World
 633 Scientific Publ. Co., River Edge, NJ, USA, 504 pp., 2001.
- 634
- 635 Manuilova, R. O., Gusev, O. A., Kutepov, A. A., von Clarmann, T., Oelhaf, H., Stiller, G. P.,
 636 Wegner, A., Lopez-Puertas, M., Martin-Torres, F. J., Zaragoza, G., and Flaud, J.-M.: Modelling
 637 of non-LTE limb spectra of i.r. ozone bands for the MIPAS space experiment, *J. Quant.*
 638 *Spectrosc. Rad. Transf.*, 59, 405-422, [https://doi.org/10.1016/S0022-4073\(97\)00120-9](https://doi.org/10.1016/S0022-4073(97)00120-9), 1998.
- 639
- 640 Mertens, C. J., Mlynchak, M. G., Lopez-Puertas, M., and Remsberg, E. E.: Impact of non-LTE
 641 processes on middle atmospheric water vapor retrievals from simulated measurements of 6.8 μm
 642 Earth limb emission, *Geophys. Res. Lett.*, 29 (9), 2-1 to 2-4,
 643 <https://doi.org/10.1029/2001GL014590>, 2002.
- 644
- 645 Mlynchak, M. G. and Drayson, R.: Calculation of infrared limb emission by ozone in the
 646 terrestrial middle atmosphere 2. Emission calculations, *J. Geophys. Res.*, 95, 16,513-16,521,
 647 <https://doi.org/10.1029/JD095iD10p16513>, 1990.
- 648



- 649 Remsberg, E., and Lingenfelser, G.: LIMS Version 6 Level 3 dataset, NASA-TM-2010-216690,
 650 available at <http://www.sti.nasa.gov> (last access: 17 September 2019), 13 pp., 2010.
- 651
- 652 Remsberg, E. E., Russell, J. M., III, Gille, J. C., Bailey, P. L., Gordley, L. L., Planet, W. G., and
 653 Harries, J. E.: The validation of Nimbus 7 LIMS measurements of ozone, *J. Geophys. Res.*, 89,
 654 5161-5178, doi:10.1029/JD089iD04p05161, 1984.
- 655
- 656 Remsberg, E. E., Gordley, L. L., Marshall, B. T., Thompson, R. E., Burton, J., Bhatt, P., Harvey,
 657 V. L., Lingenfelser, G., Natarajan, M.: The Nimbus 7 LIMS version 6 radiance conditioning and
 658 temperature retrieval methods and results, *J. Quant. Spectros. Rad. Transf.*, 86, 395-424,
 659 doi:10.1016/j.jqsrt.2003.12.007, 2004.
- 660
- 661 Remsberg, E., Lingenfelser, G., Natarajan, M., Gordley, L., Marshall, B. T., and Thompson, E.:
 662 On the quality of the Nimbus 7 LIMS version 6 ozone for studies of the middle atmosphere, *J.*
 663 *Quant. Spectros. Rad. Transf.*, 105, 492-518, doi:10.1016/j.jqsrt.2006.12.005, 2007.
- 664
- 665 Remsberg, E. E., Marshall, B. T., Garcia-Comas, M., Krueger, D., Lingenfelser, G. S., Martin-
 666 Torres, J., Mlynczak, M. G., Russell III, J. M., Smith, A. K., Zhao, Y., Brown, C., Gordley, L.
 667 L., Lopez-Gonzalez, M. J., Lopez-Puertas, M., She, C. Y., Taylor, M. J., and Thompson, E.:
 668 Assessment of the quality of the Version 1.07 temperature versus pressure profiles of the middle
 669 atmosphere from TIMED/SABER, *J. Geophys. Res.*, 113, D17101,
 670 <https://doi.org/10.1029/2008JD010013>, 2008.
- 671
- 672 Remsberg, E. E., Natarajan, M., Lingenfelser, G. S., Thompson, R. E., Marshall, B. T., and
 673 Gordley, L. L.: On the quality of the Nimbus 7 LIMS Version 6 water vapor profiles and
 674 distributions, *Atmos. Chem. Phys.*, 9, 9155-9167, www.atmos-chem-phys.net/9/9155/2009/,
 675 2009.



676

677 Remsberg, E., Natarajan, M., Marshall, B. T., Gordley, L. L., Thompson, R. E., and
678 Lingenfelser, G. S.: Improvements in the profiles and distributions of nitric acid and
679 nitrogen dioxide with the LIMS version 6 dataset, *Atmos. Chem. Phys.*, 10, 4741–4756,
680 www.atmos-chem-phys.net/10/4741/2010/, 2010.

681

682 Remsberg, E., Natarajan, M., Fairlie, T. D., Wargan, K., Pawson, S., Coy, L., Lingenfelser, G.,
683 and Kim, G.: On the inclusion of Limb Infrared Monitor of the Stratosphere version 6 ozone in a
684 data assimilation system, *J. Geophys. Res.*, 118, 7982–8000, <https://doi.org/10.1002/jgrd.50566>,
685 2013.

686

687 Roewe, D. A., Gille, J. C., and Bailey, P. L.: Infrared limb scanning in the presence of horizontal
688 temperature gradients: an operational approach, *Appl. Opt.*, 21, 3775–3783,
689 <http://dx.doi.org/10.1364/AO.21.003775>, 1982.

690

691 Rong, P. P., Russell III, J. M., Mlynczak, M. G., Remsberg, E. E., Marshall, B. T., Gordley, L.
692 L., and Lopez-Puertas, M.: Validation of Thermosphere Ionosphere Mesosphere Energetics and
693 Dynamics/Sounding of the Atmosphere using Broadband Emission Radiometry
694 (TIMED/SABER) v1.07 ozone at 9.6 μm in altitude range 15–70 km, *J. Geophys. Res.*, 114,
695 D04306, <https://doi.org/10.1029/2008JD010073>, 2009.

696

697 Sakazaki, T., Fujiwara, M., Mitsuda, C., Imai, K., Manago, N., Naito, Y., Nakamura, T.,
698 Akiyoshi, H., Kinnison, D., Sano, T., Suzuki, M., and Shiotani, M.: Diurnal ozone variations in
699 the stratosphere revealed in observations from the Superconducting Submillimeter-Wave Limb-
700 Emission Sounder (SMILES) on board the International Space Station (ISS), *J. Geophys. Res.*,
701 118, 2991–3006, <https://doi.org/10.1002/jgrd.50220>, 2013.



702

703 Shepherd, T. G., Plummer, D. A., Scinocca, J. F., Hegglin, M. I., Fioletov, V. E., Reader, M. C.,
 704 Remsberg, E., von Clarmann, T., and Wang, H. J.: Reconciliation of halogen-induced ozone loss
 705 with the total-column record, *Nature Geoscience*, 7, 443-449, doi:10.1038/ngeo2155, 2014.

706

707 Solomon, S., Kiehl, J. T., Kerridge, B. J., Remsberg, E. E., and Russell III, J. M.: Evidence for
 708 nonlocal thermodynamic equilibrium in the ν_3 mode of mesospheric ozone, *J. Geophys. Res.*,
 709 91, 9865-9876, <https://doi.org/10.1029/JD091iD09p09865>, 1986.

710

711 SPARC: The SPARC Data Initiative: Assessment of stratospheric trace gas and aerosol
 712 climatologies from satellite limb sounders, Hegglin, M. I. and Tegtmeier, S., (Eds.), SPARC
 713 Report No. 8, WCRP-5/2017, <http://www.sparc-climate.org/publications/sparc-reports/>, 2017.

714

715 Sun, C.-R., and Leovy, C.: Ozone variability in the equatorial middle atmosphere, *J. Geophys.*
 716 *Res.*, 95, 13,829-13,849, <https://doi.org/10.1029/JD095iD09p13829>, 1990.

717

718 Tegtmeier, S., Hegglin, M. I., Anderson, J., Bourassa, A., Brohede, S., Degenstein, D.,
 719 Froidevaux, L., Fuller, R., Funke, B., Gille, J., Jones, A., Kasai, Y., Krüger, K., Kyrölä, E.,
 720 Lingenfelser, G., Lumpe, J., Nardi, B., Neu, J., Pendlebury, D., Remsberg, E., Rozanov, A.,
 721 Smith, L., Toohey, M., Urban, J., von Clarmann, T., Walker, K. A. and Wang, R. H. H.: SPARC
 722 Data Initiative: A comparison of ozone climatologies from international satellite limb sounders,
 723 *J. Geophys. Res.*, 118, 12,229-12,247, doi:10.1002/2013JD019877, 2013.

724

725 WOUDC, World Ozone and Ultraviolet Radiation Data Centre, <https://woudc.org/home.php>.

726



727

728

Table 1

729

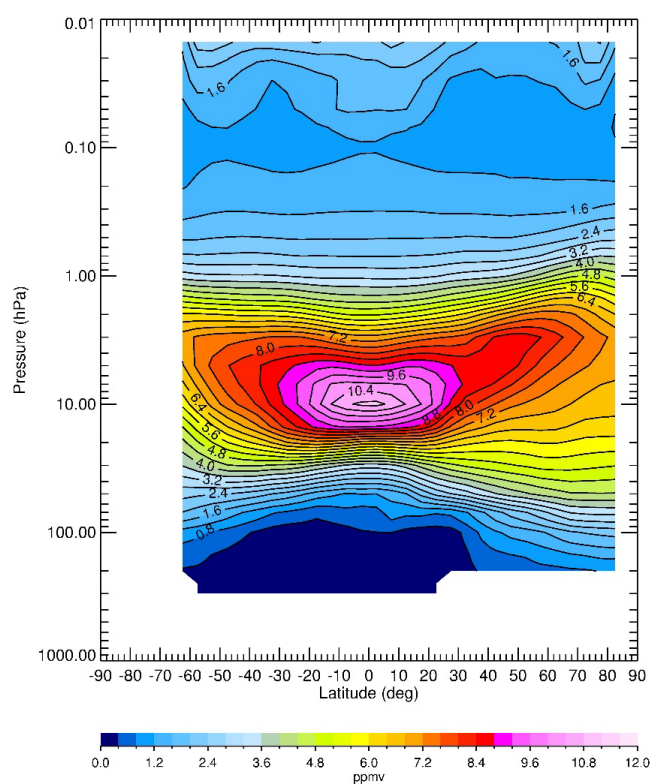
Estimates of Species Errors Due to Temperature Biases

730

Pressure (hPa)	100	50	10	3	1	0.4	0.1
Temperature Bias (K)	1.1	1.3	1.0	1.6	2.4	2.5	2.3
Ozone (%)	20	20	11	10	12	16	16
Water vapor (%)	16	18	8	15	--	--	--
Nitric acid (%)	5	1	1	6	--	--	--
T(p) Diff (V6-BC) (K)	--	1.4	1.7	-4.4	-1.6	3.1	--

731

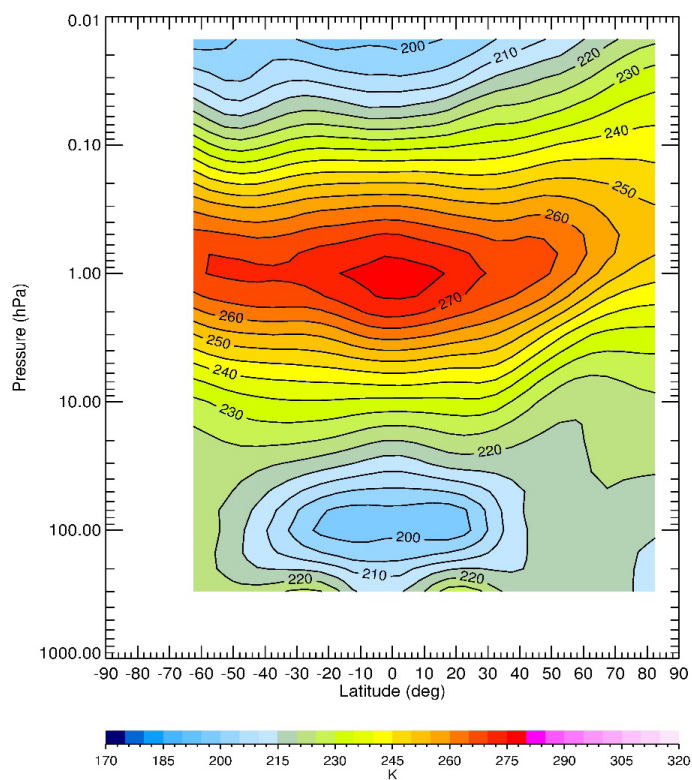
732



736
 737 Figure 1—Zonal average ozone for March 1979 from the combination of the LIMS V6
 738 ascending and descending orbital data. Contour interval (CI) is 0.4 ppbv.
 739



740



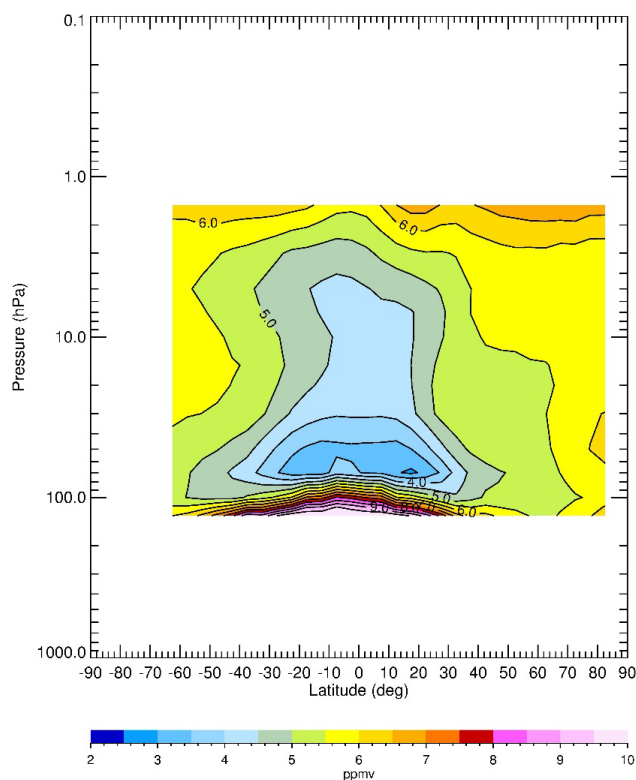
741

742 Figure 2—Zonal average temperature for March 1979. CI is 5 K.

743



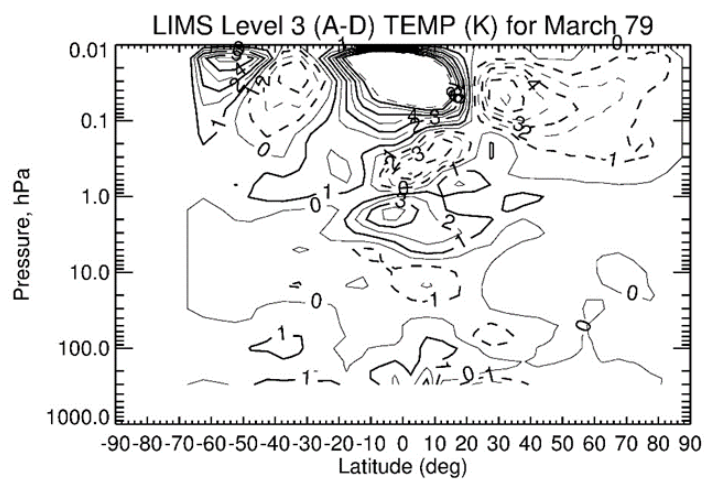
744



745

746 Figure 3—Zonal average water vapor for March 1979. CI is 0.5 ppmv.

747



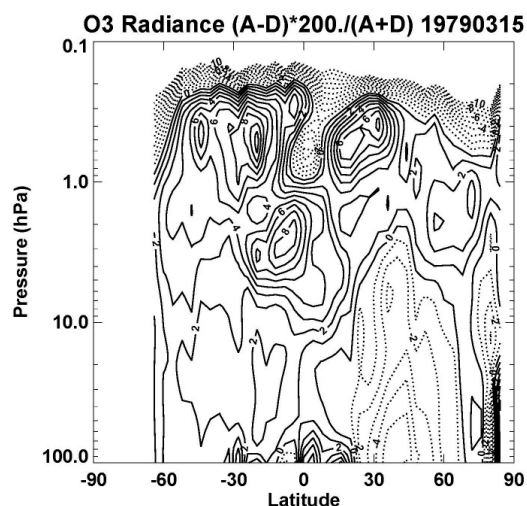
748

749 Figure 4—LIMS V6 Level 3 ascending minus descending (A-D) temperature differences (in K)
 750 for March 1979. CI is 1 K and solid contours show positive differences.

751



752



753

754 Figure 5—Ascending minus descending ozone radiance differences (in %) for March 15, 1979.

755 Contour interval is 1%.

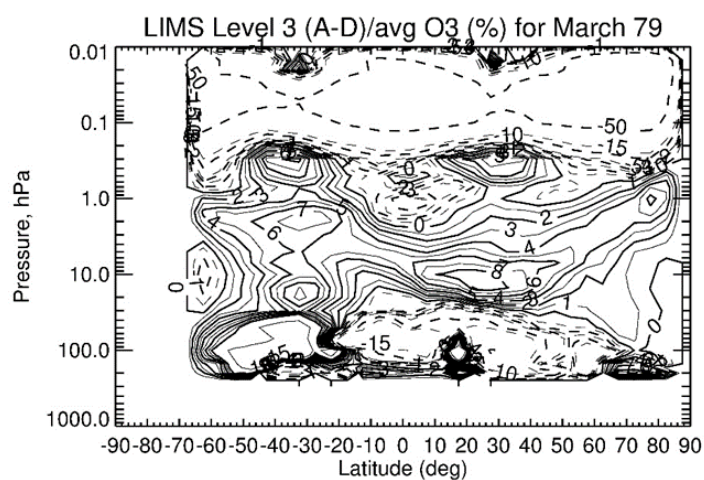
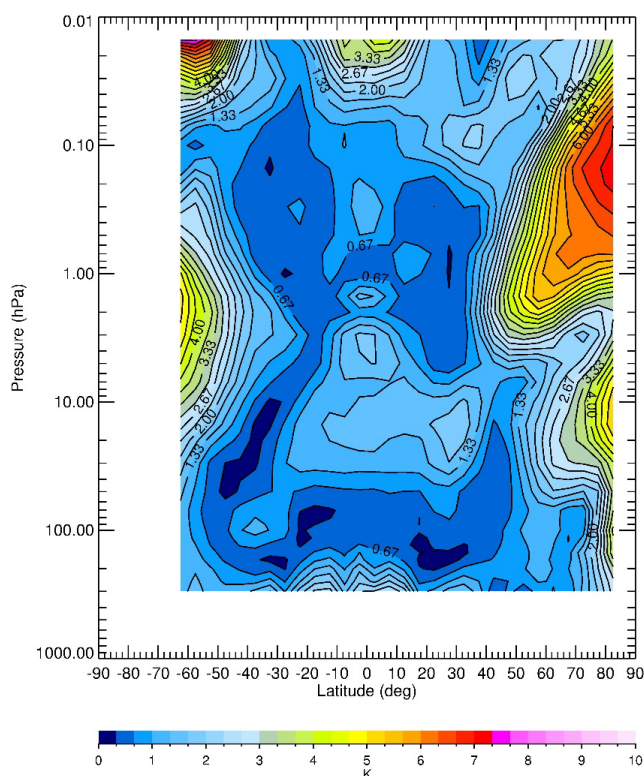


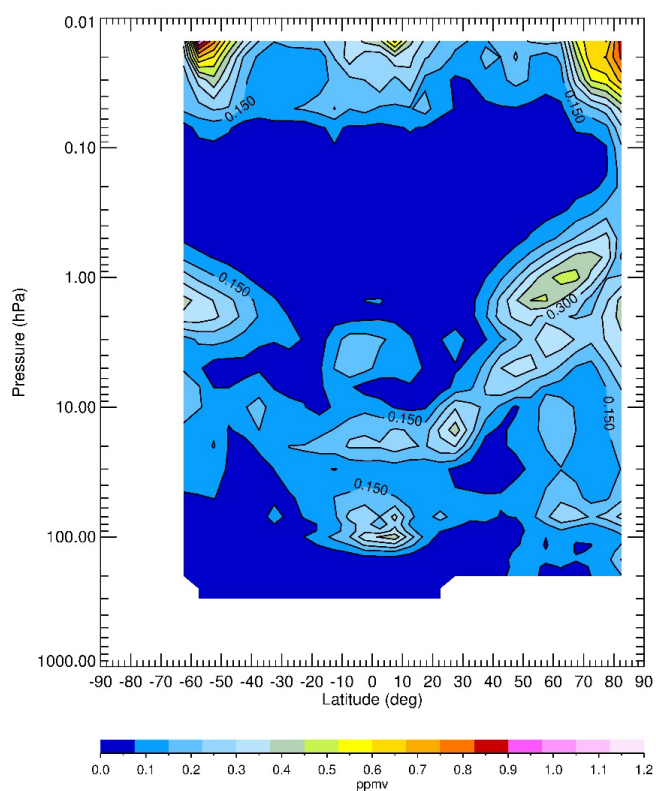
Figure 6—LIMS V6 Level 3 monthly zonal mean (A-D) ozone differences divided by average
 ozone (and given in %) for March 1979. Solid contours are positive and CI is 1% from 0 to 10,
 5% from 10 to 15, and then skipping to the 50% contour.



764

765 Figure 7—Average zonal (wave) standard deviation of temperature for March 1979. Contour
 766 interval is 0.33 K.

767



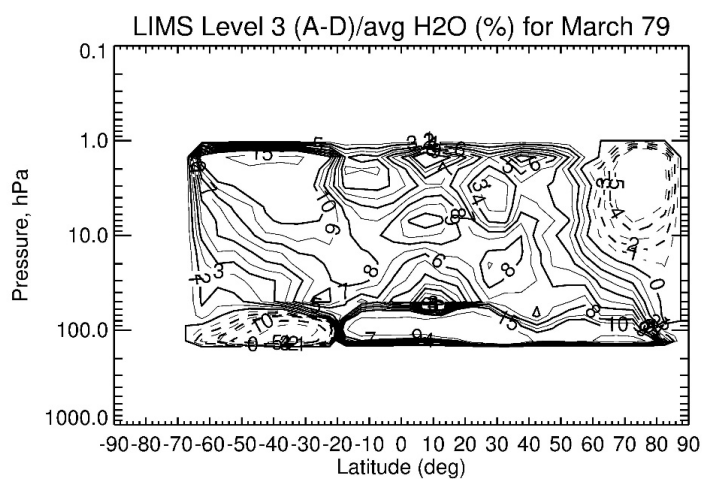
768

769 Figure 8—Average zonal (wave) standard deviation of ozone for March 1979. Contour interval
 770 is 0.075 ppmv.

771



772



773

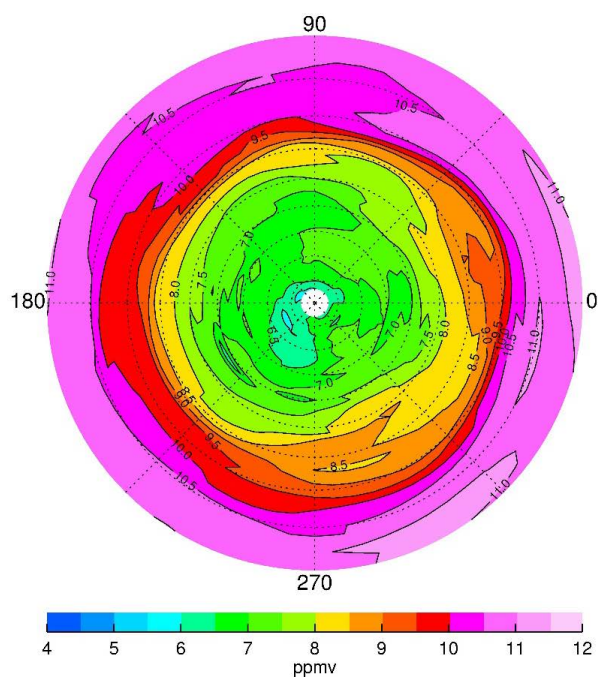
774 Figure 9—LIMS V6 Level 3 ascending minus descending (A-D) H₂O differences divided by
 775 average H₂O (and given in %) for March 1979. CI is 2% from 0 to 10 and then 5% from 10 to
 776 15; solid contours show positive differences.

777



778

779



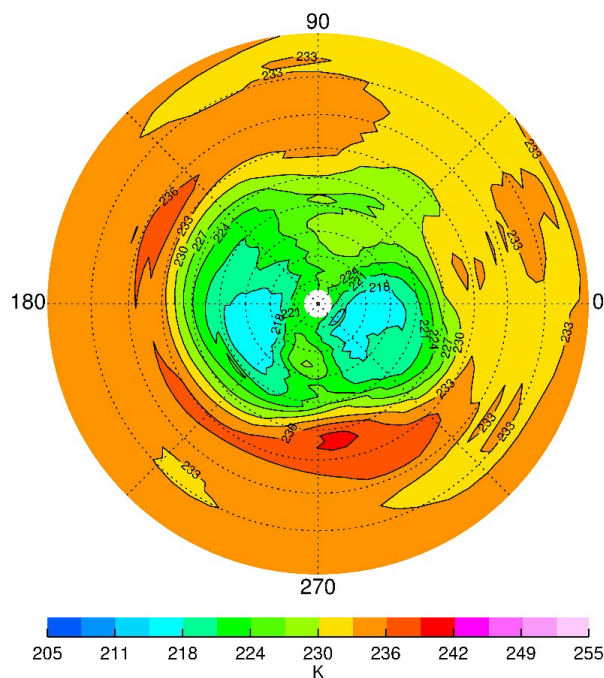
780

781 Figure 10—V6 ozone at 10 hPa for March 15, 1979, in the NH. Ozone contour interval is 0.5
 782 ppmv, and latitude spacing (dotted circles) is 10°.

783



784



785

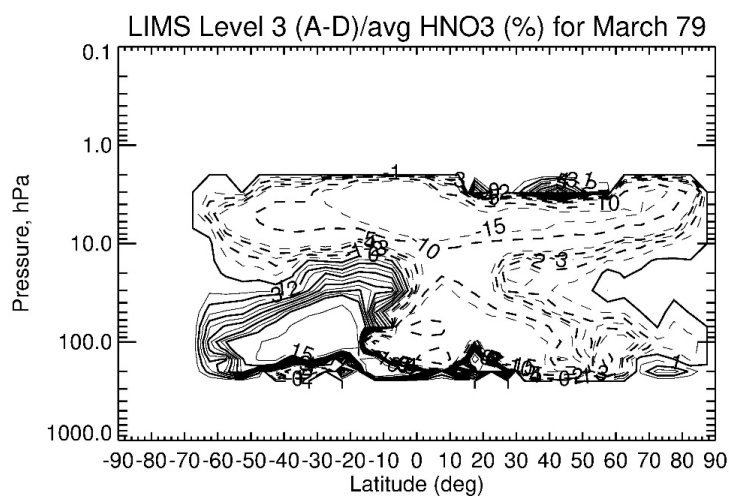
786 Figure 11—V6 temperature at 10 hPa for March 15, 1979, in the NH; contour interval is 3 K.

787

788



789



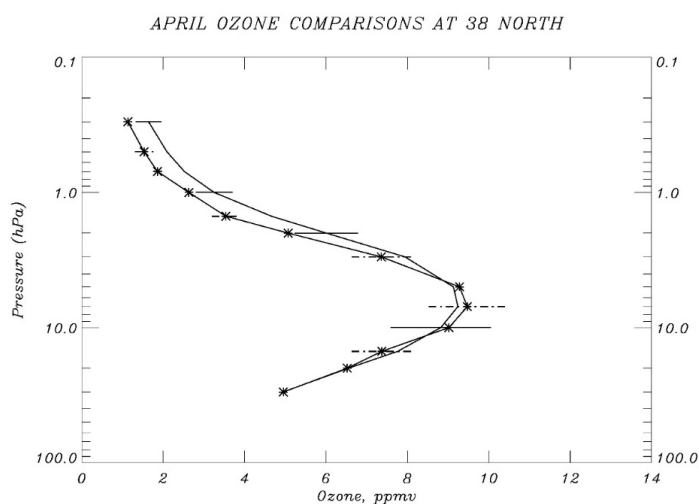
790

791 Figure 12—LIMS V6 Level 3 ascending minus descending (A-D) HNO_3 differences divided by
 792 average HNO_3 (and given in %) for March 1979. CI is 1% from 0 to 10 and then 5% from 10 to
 793 15; solid contours show positive differences.

794



795



796

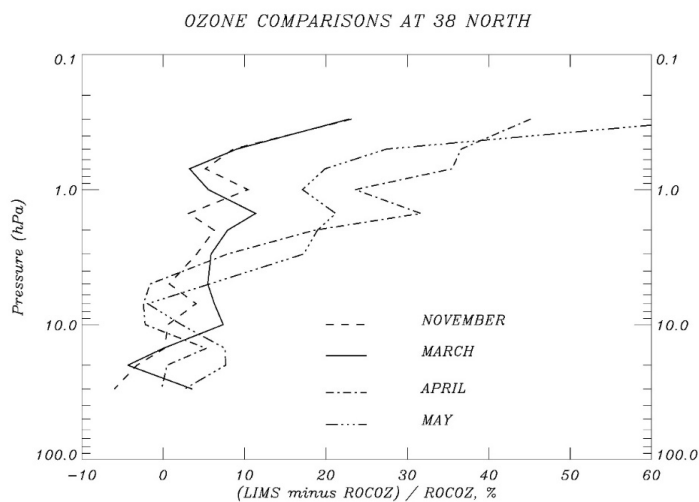
797

798 Figure 13—LIMS V6 monthly zonal mean daytime ozone (solid) for April 1979 at 38°N
 799 compared with an average of three soundings (*) at Wallops Island, VA, 38°N, in April of 1976-
 800 1978. Horizontal bars are error estimates for LIMS (solid) and for a ROCOZ sounding (dashed).

801



802



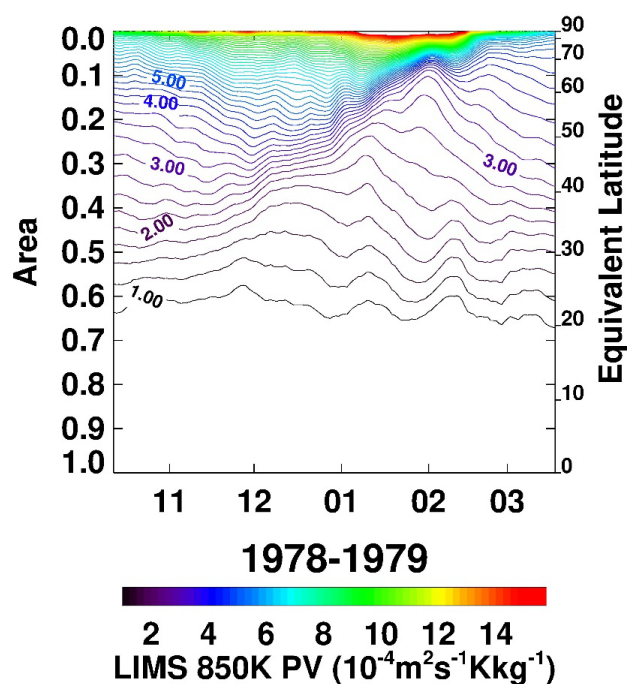
803

804 Figure 14—Monthly zonal mean V6 daytime ozone minus ROCOZ ozone (in %) for four months
 805 at 38°N.

806



807



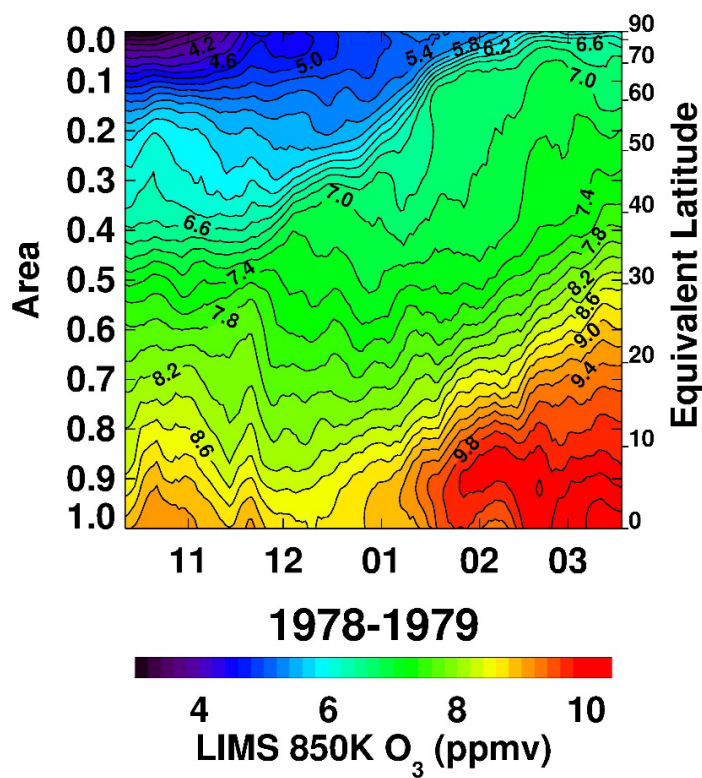
808

809 Figure 15—Area diagnostic plot of time series of NH potential vorticity (PV) contours on the
 810 850 K potential temperature surface for comparison with Butchart and Remsberg (1986, their
 811 Figure 4). PV comes from LIMS V6 Level 3 geopotential height and temperature data. Contour
 812 interval (CI) is 0.25 PV units (units of PV are $10^{-4} \text{ m}^2 \text{ s}^{-1} \text{ K kg}^{-1}$). Tic marks on the abscissa
 813 denote the 15th of each month.

814



815



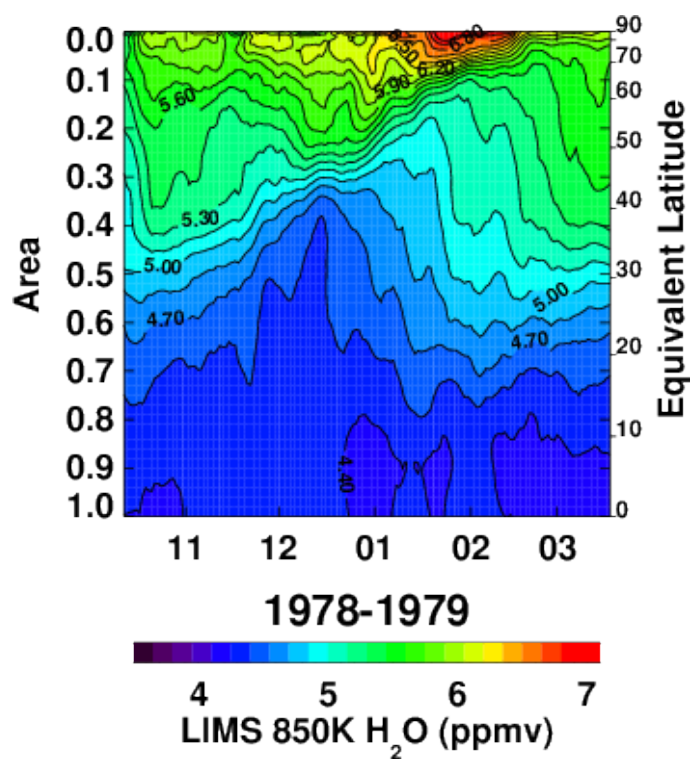
816

817 Figure 16—Area diagnostic plot of V6 Level 3 ozone for comparison with Figure 15. Ozone
 818 contour interval is 0.2 ppmv. Tick marks on the abscissa indicate the 15th of each month.

819



820



821

822 Figure 17—As in Fig. 16, but for V6 H₂O at 850 K; contour interval is 0.15 ppmv.

823